NANO LETTERS

pubs.acs.org/NanoLett Letter

Reconfigurable Photon Sources Based on Quantum Plexcitonic Systems

Jia-Bin You,# Xiao Xiong,# Ping Bai, Zhang-Kai Zhou, Ren-Min Ma, Wan-Li Yang, Yu-Kun Lu, Yun-Feng Xiao, Ching Eng Png, Francisco J. Garcia-Vidal,* Cheng-Wei Qiu,* and Lin Wu*

Cite This: *Nano Lett.* 2020, 20, 4645−4652 Read Online

ABSTRACT: A single photon in a strongly nonlinear cavity is able to block the transmission of a second photon, thereby converting incident coherent light into antibunched light, which is known as the photon blockade effect. Photon antipairing, where only the entry of two photons is blocked and the emission of bunches of three or more photons is allowed, is based on an unconventional photon blockade mechanism due to destructive interference of two distinct excitation pathways. We propose quantum plexcitonic systems with moderate nonlinearity to generate both antibunched and antipaired photons. The proposed plexcitonic systems benefit from subwavelength field localizations that make quantum emitters spatially distinguishable, thus enabling a reconfigurable photon source between antibunched and antipaired states via tailoring the energy bands. For a realistic nanoprism plexcitonic system, chemical and optical schemes of reconfiguration are demonstrated. These results pave the way to realize reconfigurable nonclassical photon sources in a simple quantum plexcitonic platform.

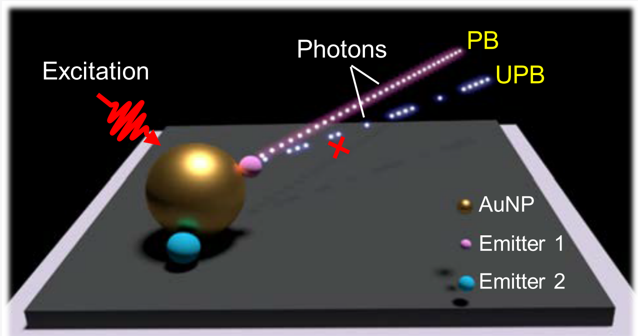

KEYWORDS: *Plexcitonic, photon blockade (PB), unconventional photon blockade (UPB), correlation functions, reconfiguration, antibunching*

INTRODUCTION

Generation and manipulation of nonclassical light lie at the heart of quantum science and technology.[1−4] Conventionally, such single photon sources can be realized when a quantum emitter is strongly coupled to a cavity, in which the optical nonlinearity is present at a single photon level. The resulting energy levels form the anharmonic Jaynes−Cummings ladder, which gives rise to conventional photon blockade (PB). In PB, an emitter in a cavity effectively modifies the cavity resonance after a single photon is absorbed, preventing subsequent photons to pass through and creating an antibunched single photon stream. This PB effect has been realized in quantum dot-cavity systems,[5] spin ensemble-cavity systems,[6,7] Kerr-nonlinearity cavities,[8] transmission line resonators,[9] and optomechanical systems.[10] The signature of PB is usually observed by measuring the second-order correlation function at zero delay $g^{(2)}(0)$. The value of $g^{(2)}(0) < 1$, manifesting a sub-Poissonian photon statistics, indicates that the system is in PB regime.

Recently, an alternative route is found to achieve photon blockade for generating nonclassical light in cavity quantum electrodynamic systems.[11−15] It is predicted that the "strong coupling" condition to attain PB could be relaxed if more than one cavity or emitter is employed.[16,17] This new mechanism, known as unconventional photon blockade (UPB), relies on the destructive quantum interference between different excitation pathways.[18,19] The UPB should be jointly characterized by the second- and third-order correlation functions at zero delay, which requires $g^{(2)}(0) < 1$ and $g^{(3)}(0) > 1$. Unlike the conventional PB, UPB suppresses the emission of two photons only and allows the emission of single photon, as well as bunches of three or more photons simultaneously. The realization of UPB has been extensively proposed in optomechanical systems,[20] quantum dot-cavity systems,[21] Kerr-nonlinearity cavities,[22] and weakly nonlinear photonic molecules.[23] In light of these efforts, UPB could not only advance the development of single photon sources but also enable the multiphoton emission that probably unveils richer physics.[17]

In this work, we explore the possibility to realize both photon blockade effects in the same Jaynes−Cummings type of quantum plexcitonic system and, more interestingly, to switch between PB and UPB freely. Plexcitons refer to polaritonic

Received: April 12, 2020
Revised: April 30, 2020
Published: May 4, 2020

https://dx.doi.org/10.1021/acs.nanolett.0c01562
Nano Lett. 2020, 20, 4645−4652

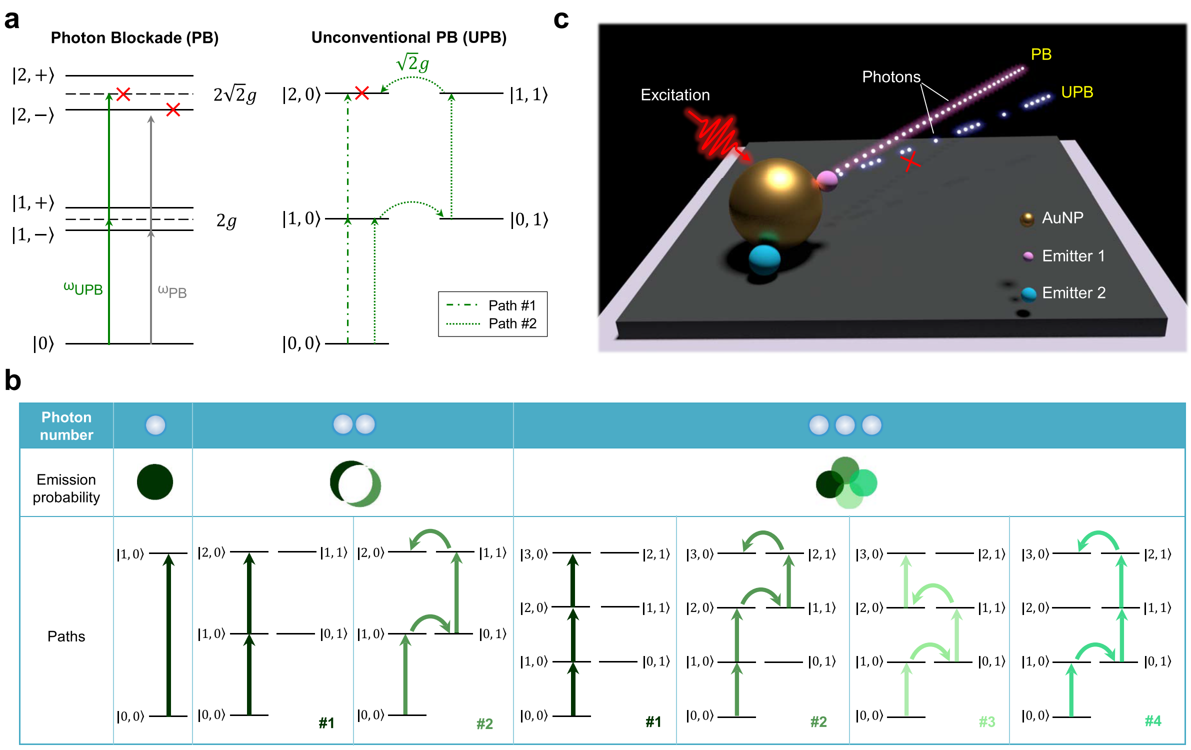

Figure 1. Quantum plexcitonic system for a reconfigurable single photon source. (a) Energy level diagram showing a two-level quantum emitter coupled to a cavity field in resonance, with coupling rate g. The suppression of two-photon emission is due to the anharmonic Jaynes–Cummings ladder for photon blockade (PB) and the destructive interference of two distinct excitation pathways for unconventional photon blockade (UPB). (b) Detailed excitation pathway analysis of UPB for one-, two-, and three-photon emission. (c) Schematics of the proposed quantum plexcitonic system for a reconfigurable single photon source between PB (antibunched) and UPB (antipaired) states.

modes that result from coherent coupling between plasmons and excitons. Three individual experiments on different plexcitonic systems[24−26] have concurrently confirmed that room-temperature strong coupling between a single quantum emitter and a single plasmonic cavity is indeed feasible with reported coupling rates of 120 meV,[24] 90 meV,[25] and 78 meV,[26] respectively. These experiments at a single emitter level successfully push plasmonics into the quantum regime, where the anharmonic energy structure is now in action as illustrated in Figure 1a, making PB highly feasible. Recently, the second-order correlation function of the photon emission statistics has been measured at room temperature by coupling a single molecule with a plasmonic nanocavity, varying from $g^{(2)}(0)$ = 0.4 to 1.45.[27] Using Hanbury, Brown, and Twiss interferometry, nonclassical emission showing clear evidence of antibunching ($g^{(2)}(0) < 1$) has also been observed from one to three semiconductor quantum dots within plasmonic silver-bowtie cavities.[28] Moreover, UPB is also readily achievable in such a plexcitonic system by carefully engineering the quantum interference between different excitation pathways for multiple photons. Taking the two-photon case as an example elaborated in Figure 1b, two distinct excitation pathways (i.e., path #1: |0, 0⟩ → |1, 0⟩ → |2, 0⟩ and path #2: |0, 0⟩ → |1, 0⟩ → |0, 1⟩ → |1, 1⟩ → |2, 0⟩) could destructively interfere, and thus, the two-photon emission is suppressed. Here, |i, j⟩ represents a plexcitonic state, where i and j correspond to the number of plasmons and excitons, respectively.

Our proposed quantum plexcitonic system is schematically illustrated in Figure 1c, which operates as a reconfigurable single photon source driven by coherent light of frequency ω. The plexcitonic system consists of a plasmonic nanocavity (resonant energy ω_c, decay rate κ) and distinguishable quantum emitters (transition energy ω_{e1} or ω_{e2}, decay rate γ_{e1} or γ_{e2}) with coupling rate of g_{e1} or g_{e2} to the plasmonic cavity. By carefully designing this plexcitonic system, we are able to realize either PB or UPB effect. As shown in Figure 1c, PB generates antibunched single photon beam, whereas UPB generates antipaired photons with certain probability to emit bunched photons of three or more. It should be noted that a spherical Au nanoparticle is drawn in Figure 1c for illustration purpose only. In practice, plasmonic nanocavities offering strong field localization, such as bowtie,[24,28] NP-on-mirror,[25,27,29] cuboid Au@Ag nanorod,[26] or nanoprism,[30,31] would be more feasible.

■ RESULTS AND DISCUSSIONS

A full quantum mechanical description based on the Lindblad master equation is used to describe the quantum emitter, plasmonic cavity, and the interaction between them.[32,33] We then analyze the equal-time second- and third-order correlations of the cavity field (see SI-1) to quantify the photon blockade effects. In modern quantum optics, the equal-time correlation function $g^{(n)}(\tau = 0)$ has been employed as a criterion to characterize the statistical and coherent properties of a light source, where n is the order of the correlation function and τ is the time delay.[14,17] For $g^{(n)}(0) > 1$, $g^{(n)}(0) = 1$, or $g^{(n)}(0) < 1$, the n-photons are bunching, coherent, or antibunching, following super-Poissonian, Poissonian, or sub-Poissonian statistics, respectively. By comparing any light source against a coherent light source with Poissonian distribution, it can be known that the n-photon emission is enhanced when $g^{(n)}(0) > 1$ (classical light) and suppressed

https://dx.doi.org/10.1021/acs.nanolett.0c01562
Nano Lett. 2020, 20, 4645−4652

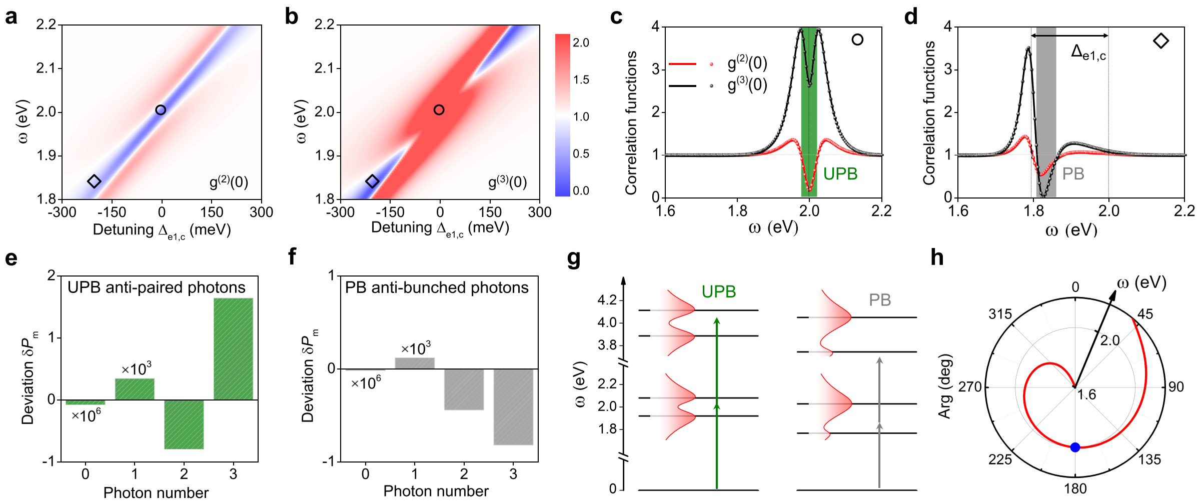

Figure 2. Plexcitonic systems with indistinguishable emitters. (a, b) The effect of the detuning between the emitter and the cavity $\Delta_{e1,c}$ on the correlation functions at zero delay $g^{(2)}(0)$ and $g^{(3)}(0)$. Symbol "circle" denotes a resonant system with UPB effect. Symbol "diamond" denotes an off-resonant system with PB effect. (c, d) The two representative plexcitonic systems denoted by circle and diamond: (c) antipaired photon source based on UPB with $\Delta_{e1,c} = 0$ and (d) antibunched photon source based on PB with $\Delta_{e1,c} = -205$ meV. The lines and the dots are the simulation results from the Lindblad master equation and the analytic solutions from the equations-of-motion method, respectively. (e, f) Photon statistics, showing suppressed or enhanced m-photon emission probability for the plexcitonic systems in (c) and (d), respectively. (g) Calculated energy level diagrams, overlapped with the extinction spectra representing the density of states, for the plexcitonic systems in (c) and (d). (h) The phase difference $\delta\theta$ between the interference pathways for the UPB system in (c). In present study, $\omega_c = 2$ eV, $\kappa = 350$ meV, $\gamma_{e1} = 80$ meV, and $g_{e1} = 80$ meV are fixed; ω_{e1} is the variable.

when $g^{(n)}(0) < 1$ (quantum light). For instance, the measured second-order photon correlation curves $g^{(2)}(\tau)$ of light emitted from a single quantum dot within a silver bowtie indicates antibunching in the correlation curve at zero delay, with a value lower than 0.5.[28] In this work, we focus on such nonclassical photon sources with $g^{(2)}(0) < 1$ but employ $g^{(3)}(0)$ to further differentiate PB and UPB mechanisms. Specifically, we use the criterion of $g^{(2)}(0) < 1$ and $g^{(3)}(0) < 1$ to indicate the conventional PB with sub-Poissonian photon distribution. On the other hand, $g^{(2)}(0) < 1$ but $g^{(3)}(0) > 1$ defines the UPB,[14,17,19] where two-photon emission is suppressed but the enhanced third-order correlation implies the emission of multiple photons.

Plexcitonic Systems with Indistinguishable Emitters. We start our discussions with a plexcitonic system with indistinguishable emitters (notated as e_1), meaning that any additional emitters are identical. In our study, the plasmonic cavity ($\omega_c = 2$ eV, $\kappa = 350$ meV) and the decay rate of emitter $\gamma_{e1} = 80$ meV are fixed unless otherwise stated. In general, we can set the state of this cavity-e_1 plexcitonic system by adjusting the detuning $\Delta_{e1,c} = \omega_{e1} - \omega_c$ or the coupling rate g_{e1} between the plasmonic cavity and the emitter. As an example, only the effect of energy detuning $\Delta_{e1,c}$ will be analyzed here. Figures 2a and 2b present $g^{(2)}(0)$ and $g^{(3)}(0)$ for plexcitonic systems bearing the same coupling rate of $g_{e1} = 80$ meV but various detunings $\Delta_{e1,c}$. Areas of both $g^{(2)}(0) < 1$ and $g^{(3)}(0) < 1$ indicate the conventional PB, and areas of $g^{(2)}(0) < 1$ but $g^{(3)}(0) > 1$ define UPB. Interestingly, photon blockade is always observed in a narrow blue/red region when the probing frequency ω is close to the frequency of emitter because the nonlinearity of our plexcitonic system arises from the quantum emitter. Otherwise, when ω is far away from the frequency of emitter, only the coherent light can be observed, i.e., the white-color regions with $g^{(2)}(0) = 1$ and $g^{(3)}(0) = 1$.

Among all the systems bearing the same coupling rate of $g_{e1} = 80$ meV shown in Figures 2a and 2b, a resonant system (circle symbol) manifests the feature of UPB, while an off-resonant system (diamond symbol) with detuning $|\Delta_{e1,c}| > 100$ meV enters into the PB region. These two representative systems are illustrated in Figures 2c and 2d. For the UPB antipaired system shown in Figure 2c, two-photon emission is suppressed ($g^{(2)}(0) < 1$), whereas three or more photons emit cooperatively ($g^{(3)}(0) > 1$), when driven by a laser of energy around $\omega = 2$ eV. The other system in Figure 2d, with a detuning of $\Delta_{e1,c} = -205$ meV, will support PB at a different laser energy around $\omega = 1.82$ eV, where the photon is emitted one after another antibunchingly with $g^{(2)}(0) < 1$ and $g^{(3)}(0) < 1$. Besides, there is another interesting peak at 1.78 eV, accounting for the photon bunching regime[34] for the multilevel plexcitonic system.

To illustrate the suppression and enhancement of m-photon emission unambiguously, we also analyze the photon statistics (see SI-2) and present the photon-number distribution $P = \{P_m|m = 0, 1, 2, ...\}$ in Figures 2e and 2f, for the two representative plexcitonic systems in Figures 2c and 2d. In the context of a lossy plexcitonic system, when the population of m-photons P_m is suppressed (or enhanced), i.e., $\delta P_m < 0$ (or >0), the m-th order correlation is simultaneously suppressed (or enhanced), i.e., $g^{(m)}(0) < 1$ (or >1). From the photon statistics shown in Figure 2e, two-photon emission is suppressed while three-photon emission is enhanced, corresponding to the characteristics of the UPB photon source. In contrast, for the other system in Figure 2f, both two-photon and three-photon emissions are suppressed, manifesting the PB feature. It is worth highlighting that this analysis of photon statistics provides a possible experimental route via photon counting experiments[35−40] to reconstruct the correlation functions for verifying our proposal.

https://dx.doi.org/10.1021/acs.nanolett.0c01562
Nano Lett. 2020, 20, 4645−4652

To explain the underlying mechanism, we plot the energy level diagrams of the above two plexcitonic systems in Figure 2g. On top of it, we also plot the calculated extinction spectra showing Rabi splitting[26] to represent the energy level broadening effect due to the finite decay rate. The energy level diagram is recovered when the decay rate is set to zero. Therefore, we use this extinction spectra to describe the number of states that are available to be occupied in the plexcitonic system around each energy level, similar to the concept of density of states (DOS) in condensed matter physics. It is interesting to note that the large decay rate of plasmonic cavity κ = 350 meV effectively creates more optical states near each energy level, even at the dip of the Rabi splitting. For the resonant UPB system driven by the laser field ω = 2 eV (green arrows), the second photon is able to enter into the second energy band and populate the energy states with certain probability. But, the photons excited via distinct pathways will interfere destructively (see Figure 2h), leading to the suppression of two-photon emission. On the other hand, for the PB off-resonant system, the energy levels are shifted downward, accompanied by the asymmetric extinction spectra. When driven by a laser with ω = 1.82 eV (gray arrows), the second photon is no longer able to enter into the second energy band, leading to PB.

Our numerical calculations can be analytically reproduced by the equations-of-motion method (see SI-3), as indicated in Figures 2c and 2d (represented by dots). This method also allows us to reveal the quantum interference mechanism for the UPB system in Figure 2c. As derived in SI-3, the two-photon population $|c_5|^2 = |A_{52}c_2 + A_{53}c_3|^2$ can be interpreted as the interference of two leading-order pathways shown in Figure 1b. The phase difference between the probability amplitudes for these two pathways $\delta\theta$ = Arg($A_{52}c_2$) − Arg($A_{53}c_3$) is plotted as a function of driven laser frequency ω in Figure 2h. At ω = 2 eV where $g^{(2)}(0)$ reaches its minimum, the two pathways are out of phase ($\delta\theta = \pi$), as indicated by the blue dot. This is the evidence of destructive interference.

Plexcitonic Systems with Distinguishable Emitters. Once we have demonstrated that a quantum plexcitonic system with indistinguishable emitters could support either PB or UPB effect, we will show how the system can become actively reconfigurable between the two effects by introducing a second type of emitter e_2 into the picture. In Figure 3, we show a proof-of-concept study on how the second emitter e_2 modifies the emission property of the original cavity-e_1 system. In the present study, the cavity-e_1 system is initially set into UPB state based on the resonant system ($\omega_c = \omega_{e1}$ = 2 eV) in Figure 2c. The second emitter e_2 has a fixed decay rate of γ_{e2} = 60 meV, whereas g_{e2} and ω_{e2} are the variables. Figure 3a maps out $g^{(2)}(0)$ and $g^{(3)}(0)$ as a function of the detuning between e_2 and the cavity $\Delta_{e2,c} = \omega_{e2} - \omega_c$, when e_2 is coupled to the cavity with g_{e2} = 80 meV. As previously discussed, the photon blockade regions only appear when the probing frequency ω is close to the frequencies of the two emitters, as the nonlinearity of the plexcitonic system arises from the quantum emitters. With the addition of the e_2, it is observed that PB can now be realized in the near-resonant blue islands highlighted by the dashed rectangles.

To elaborate the reconfiguration, in Figure 3b, we start from the antipaired UPB light source with g_{e2} = 0 in Figure 2c and show that it changes to an antibunched PB light source when e_2 with small detuning $\Delta_{e2,c}$ = 40 meV couples to the cavity

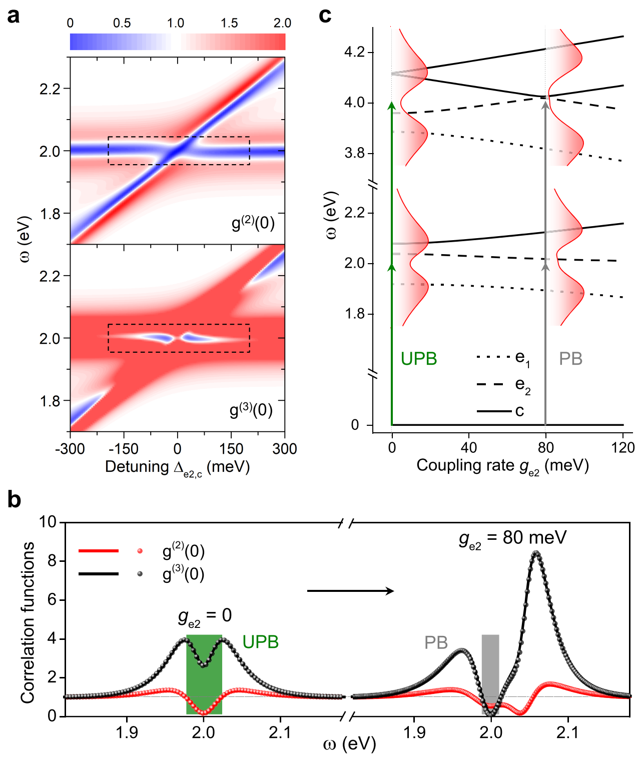

Figure 3. Plexcitonic systems with distinguishable emitters. (a) The effect of the detuning between the second emitter and the cavity $\Delta_{e2,c}$ on the correlation functions $g^{(2)}(0)$ and $g^{(3)}(0)$ for a fixed coupling rate g_{e2} = 80 meV. Dashed rectangles highlight the PB region. (b) Case study of reconfiguration from UPB antipaired to PB antibunched quantum light source by a second emitter e_2 slightly detuned from the cavity-e_1 system with $\Delta_{e2,c}$ = 40 meV. The lines and the dots are the simulation results from the Lindblad master equation and the analytic solutions from the equations-of-motion method, respectively. (c) Calculated energy level diagrams as a function of the coupling rate between e_2 and the cavity g_{e2}, with fixed $\Delta_{e2,c}$ = 40 meV. Here, the extinction spectra for g_{e2} = 0 and g_{e2} = 80 meV are provided to indicate the DOS of these two plexcitonic systems. In present study, a resonant cavity-e_1 system is employed with $\omega_c = \omega_{e1}$ = 2 eV, κ = 350 meV, γ_{e1} = 80 meV, and g_{e1} = 80 meV. The second emitter has fixed γ_{e2} = 60 meV, whereas ω_{e2} and g_{e2} are the variables.

with g_{e2} = 80 meV, driven by the same laser at ω = 2 eV. Similarly, we employ the equation-of-motion method to obtain analytic solutions of $g^{(2)}(0)$ and $g^{(3)}(0)$ for the plexcitonic system with distinguishable emitters (i.e., cavity-e_1-e_2) (see SI-3), which again agree well with those obtained from the Lindblad master equation in Figure 3b.

The PB region is found to be critically dependent on the coupling rate g_{e2}. To provide a simple physical picture, we plot the energy levels of the cavity-e_1-e_2 plexcitonic system as a function of g_{e2} in Figure 3c. With the participation of e_2, three (or four) energy levels appear for the first (or second) energy band. For the first energy band around 2 eV, the second emitter e_2 (dashed line) will increase the energy level splittings of the cavity-e_1 system (solid and dotted lines) when the perturbation becomes stronger, i.e., g_{e2} is larger. For the second energy band around 4 eV, in addition to the increased cavity-e_1 energy splitting, e_2 (dashed line) starts to strongly interact with the cavity (solid line), revealing a clear anticrossing feature near g_{e2} = 80 meV. This results in a minimum DOS, blocking the absorption of second photon for the cavity-e_1-e_2 PB system, as indicated by the gray arrows. In contrast, for the UPB

https://dx.doi.org/10.1021/acs.nanolett.0c01562
Nano Lett. 2020, 20, 4645−4652

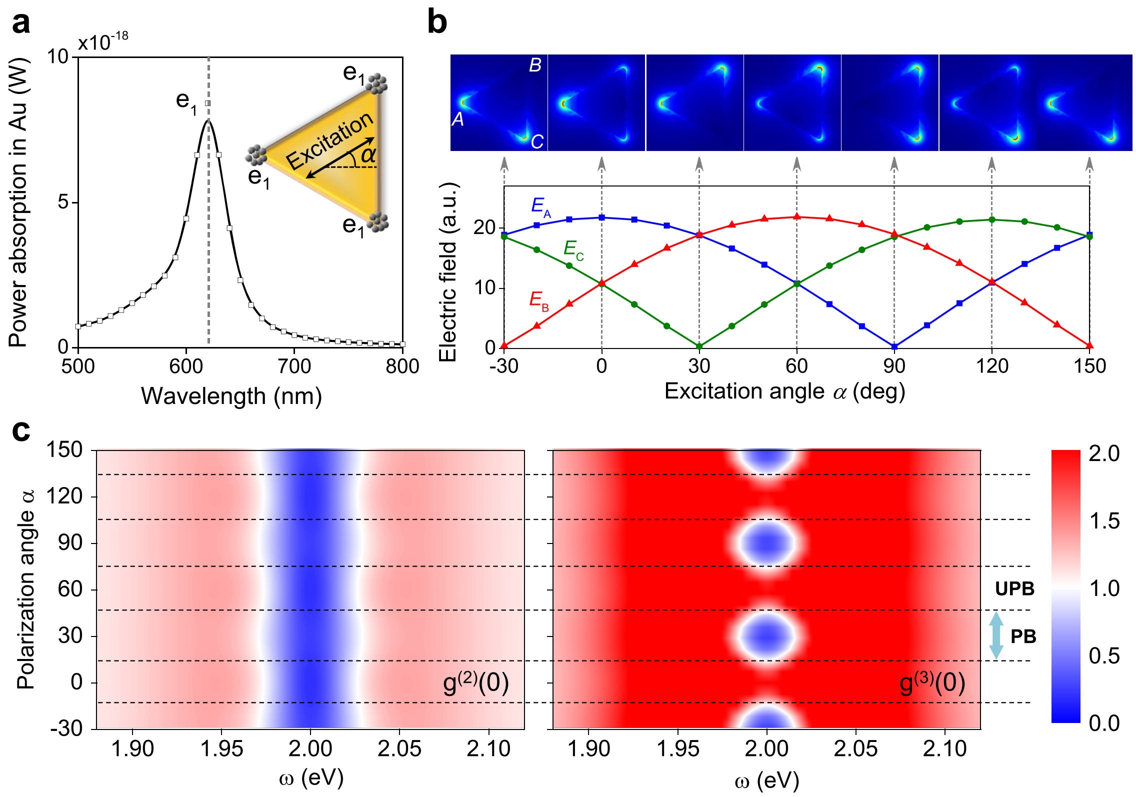

Figure 4. Optically reconfigurable single photon sources on nanoprisms. (a) The simulated absorption spectrum to identify the nanoprism plasmon mode, which is designed on resonance with the emitters e_1. Inset: schematics of the reconfigurable single photon source modulated by the polarization angle α of the incident light, in which the coupling rate between the emitters and the nanoprism is strongly dependent on the local electric field. (b) The electric field distributions of the nanoprism plasmon mode (top) and the local electric fields at the three apexes (bottom) as the polarization angle α of incident light is rotated from −30° to 150°. (c) The effect of the incident polarization angle α on the correlation functions $g^{(2)}(0)$ and $g^{(3)}(0)$, with the PB region highlighted in light blue arrow.

system with indistinguishable emitters at $g_{e2} = 0$ (green arrows), both the first and second photons occupy some optical energy states with much higher DOS.

The study above explains the mechanism to reconfigure a photon source between UPB and PB states in a plexcitonic system, when the indistinguishable quantum emitters become distinguishable during a typical reconfiguration process. It is based on a simplified quantum optics model without taking into consideration of any plasmonic cavity design. In the following, we will illustrate the reconfiguration process in a realistic plasmonic cavity.

Realistic Plexcitonic Systems. With rapid development in quantum plasmonics,[41,42] our proposal becomes experimentally feasible. The recently developed diexcitonic strong coupling system[31,43] would be an ideal experimental platform to realize the reconfigurable photon source. In particular, a potential diexcitonic strong coupling system could be photochromic spiropyran molecules,[44] whose ratios could be chemically and reversibly controlled. This chemical scheme of reconfiguration typically changes the energy of emitters, making them distinguishable (see SI-4).

Instead of changing the properties of emitters, we could externally rotate the polarization angle α of the incident light to tune the coupling rate of emitters. We elaborate the idea on a nanoprism-e_1 resonant plexcitonic system with an Au nanoprism with side length of 55 nm and a plasmon resonance at 2 eV (or 620 nm). As shown in Figure 4a, the emitters e_1 coated around the entire surface of the nanoprism are distinguished by their locations (or spatially distinguishable), where we only mark down the three apexes with huge plasmonic field enhancements: A, B, C. As the polarization angle α rotates from −30° to 150°, the electric fields at the three locations change accordingly, as vividly shown in Figure 4b. The electric fields have a direct impact on the local coupling rates,[26] which can be mathematically approximated as $g_A = 85|\cos\alpha|$, $g_B = 85|\cos(\alpha - 60°)|$, and $g_C = 85|\cos(\alpha + 60°)|$, following the same trend of E_A, E_B, and E_C in Figure 4b. These location-dependent coupling rates should be taken into the Hamiltonian, $H = \Delta_c a^\dagger a + \Delta_{A1}\sigma_{A1}^+\sigma_{A1}^- + \Delta_{B1}\sigma_{B1}^+\sigma_{B1}^- + \Delta_{C1}\sigma_{C1}^+\sigma_{C1}^- + E_l(a + a^\dagger) + g_A(a\sigma_{A1}^+ + a^\dagger\sigma_{A1}^-) + g_B(a\sigma_{B1}^+ + a^\dagger\sigma_{B1}^-) + g_C(a\sigma_{C1}^+ + a^\dagger\sigma_{C1}^-)$, where the frequencies are $\omega_c = \omega_{A1} = \omega_{B1} = \omega_{C1} = 2$ eV, representing the same type of e_1 sitting at different locations. These same type of emitters e_1 become distinguishable due to the variations of the location-dependent coupling rates. With $\kappa = 350$ meV and $\gamma_{e1} = 80$ meV, the Lindblad master equation is written as

$$\partial_t\rho = i[\rho, H] + \frac{\kappa}{2}\mathcal{D}[a]\rho + \frac{\gamma_{e1}}{2}\mathcal{D}[\sigma_{A1}^-]\rho + \frac{\gamma_{e1}}{2}\mathcal{D}[\sigma_{B1}^-]\rho + \frac{\gamma_{e1}}{2}\mathcal{D}[\sigma_{C1}^-]\rho.$$

The results of calculated $g^{(2)}(0)$ and $g^{(3)}(0)$ are shown in Figure 4c, where a repeating reconfiguration pattern of PB–UPB of a cycle of 60° are observed with the tuning polarization angle α, when driven by a laser of 2 eV in resonance with the system. The repeating cycle of 60° in the correlation function of $g^{(3)}(0)$ in Figure 4c follows the electric field distributions in

https://dx.doi.org/10.1021/acs.nanolett.0c01562
Nano Lett. 2020, 20, 4645−4652

Figure 4b, where an equivalent field distribution appears every 60°. Within each cycle of 60°, the modulation of $g^{(3)}(0)$ below and above 1 is necessary to realize the reconfiguration between UPB and PB, which can only be achieved with peak coupling rate between 80 and 100 meV.

■ CONCLUSIONS AND OUTLOOK

We have theoretically proposed a single photon source based on a quantum plexcitonic system with moderate nonlinearity. Either PB antibunched or a UPB antipaired photon source can be realized in a well-designed plexcitonic system with indistinguishable emitters. To turn the passive device active, a second type of emitters can be introduced to reconfigure the photon source between the PB and UPB states via tuning the energy bands. In other words, this category of commonly seen plexcitonic systems with distinguishable emitters are particularly useful in realizing a reconfigurable photon source. We demonstrate two realistic schemes of reconfiguration based on the same nanoprism plasmonic cavity, either chemically or optically. The chemical way directly changes the properties of the emitters, while the optical means externally varies the electric field distributions of the plasmonic cavity so as to change the coupling rate of the emitters at different locations. The latter, making emitters spatially distinguishable, is recognized as the key feature of plexcitonic systems.

From another perspective, the electromagnetic environment surrounding the plexcitonic system could influence the plasmon-emitter coupling. In a vacuum environment, the radiative-field originates from the near-field of the plexcitonic system, and as a consequence, there is no further coupling between radiative-field and near-field. However, when an external microcavity is introduced into the system, the radiative-field is now confined inside the microcavity, with its lifetime being related to the cavity quality factor. This idea leads to the concept of microcavity plasmonics,[41,45−48] in which an embedding photonic microcavity is utilized to engineer the response of plasmonic nanostructures. In this way, both the high field concentration associated with localized surface plasmons and the low damping of cavity photons could be exploited to achieve a better performance.

■ ASSOCIATED CONTENT

Supporting Information

The Supporting Information is available free of charge at https://pubs.acs.org/doi/10.1021/acs.nanolett.0c01562.

Quantum description based on the Lindblad master equation; photon statistics; equations-of-motion method; and chemical scheme of reconfiguration (PDF)

■ AUTHOR INFORMATION

Corresponding Authors

Francisco J. Garcia-Vidal − *Departamento de Fisica Teorica de la Materia Condensada and Condensed Matter Physics Center (IFIMAC), Universidad Autonoma de Madrid, E-28049 Madrid, Spain;* orcid.org/0000-0003-4354-0982; Email: fj.garcia@uam.es

Cheng-Wei Qiu − *Department of Electrical and Computer Engineering, National University of Singapore, Singapore 117583;* Email: chengwei.qiu@nus.edu.sg

Lin Wu − *Institute of High Performance Computing, Agency for Science, Technology, and Research (A*STAR), Connexis, Singapore 138632;* orcid.org/0000-0002-3188-0640; Email: wul@ihpc.a-star.edu.sg

Authors

Jia-Bin You − *Institute of High Performance Computing, Agency for Science, Technology, and Research (A*STAR), Connexis, Singapore 138632*

Xiao Xiong − *Institute of High Performance Computing, Agency for Science, Technology, and Research (A*STAR), Connexis, Singapore 138632*

Ping Bai − *Institute of High Performance Computing, Agency for Science, Technology, and Research (A*STAR), Connexis, Singapore 138632*

Zhang-Kai Zhou − *State Key Laboratory of Optoelectronic Materials and Technologies, School of Physics, Sun Yat-sen University, Guangzhou 510275, P. R. China;* orcid.org/0000-0002-4341-3097

Ren-Min Ma − *State Key Laboratory for Mesoscopic Physics and Collaborative Innovation Center of Quantum Matter, School of Physics, Peking University, Beijing 100871, P. R. China;* orcid.org/0000-0003-4199-5772

Wan-Li Yang − *State Key Laboratory of Magnetic Resonance and Atomic and Molecular Physics, Wuhan Institute of Physics and Mathematics, Chinese Academy of Sciences, Wuhan 430071, P. R. China*

Yu-Kun Lu − *State Key Laboratory for Mesoscopic Physics and Collaborative Innovation Center of Quantum Matter, School of Physics, Peking University, Beijing 100871, P. R. China*

Yun-Feng Xiao − *State Key Laboratory for Mesoscopic Physics and Collaborative Innovation Center of Quantum Matter, School of Physics, Peking University, Beijing 100871, P. R. China*

Ching Eng Png − *Institute of High Performance Computing, Agency for Science, Technology, and Research (A*STAR), Connexis, Singapore 138632*

Complete contact information is available at: https://pubs.acs.org/10.1021/acs.nanolett.0c01562

Author Contributions

[#]These two authors contributed equally.

Notes

The authors declare no competing financial interest.

■ ACKNOWLEDGMENTS

The Institute of High Performance Computing (IHPC) acknowledges financial support from the National Research Foundation Singapore (NRF2017-NRF-NSFC002-015, NRF2016-NRF-ANR002) and A*STAR SERC (A1685b0005). W.-L. Yang acknowledges financial support from the Youth Innovation Promotion Association (CAS no. 2016299). F.J. Garcia-Vidal acknowledges support by the QuantERA program of the European Commission with funding by the Spanish AEI through project PCI2018-093145, and from the Spanish Ministry of Science and Innovation, through the "María de Maeztu" Programme for Units of Excellence in R&D (CEX2018-000805-M).

■ REFERENCES

(1) Scarani, V.; Bechmann-Pasquinucci, H.; Cerf, N. J.; Dušek, M.; Lütkenhaus, N.; Peev, M. The security of practical quantum key distribution. *Rev. Mod. Phys.* **2009**, *81*, 1301−1350.

(2) Herrero-Collantes, M.; Garcia-Escartin, J. C. Quantum random number generators. *Rev. Mod. Phys.* **2017**, *89*, 015004.

(3) Pezzè, L.; Smerzi, A.; Oberthaler, M. K.; Schmied, R.; Treutlein, P. Quantum metrology with nonclassical states of atomic ensembles. *Rev. Mod. Phys.* **2018**, *90*, 035005.
(4) Chunnilall, C. J.; Degiovanni, I. P.; Kück, S.; Müller, I.; Sinclair, A. G. Metrology of single-photon sources and detectors: a review. *Opt. Eng.* **2014**, *53*, 081910.
(5) Dayan, B.; Parkins, A. S.; Aoki, T.; Ostby, E. P.; Vahala, K. J.; Kimble, H. J. A photon turnstile dynamically regulated by one atom. *Science* **2008**, *319*, 1062−1065.
(6) Sáez-Blázquez, R.; Feist, J.; Fernández-Domínguez, A.; García-Vidal, F. Enhancing photon correlations through plasmonic strong coupling. *Optica* **2017**, *4*, 1363−1367.
(7) Sáez-Blázquez, R.; Feist, J.; García-Vidal, F.; Fernández-Domínguez, A. Photon statistics in collective strong coupling: nanocavities and microcavities. *Phys. Rev. A: At., Mol., Opt. Phys.* **2018**, *98*, 013839.
(8) Imamoḡlu, A.; Schmidt, H.; Woods, G.; Deutsch, M. Strongly interacting photons in a nonlinear cavity. *Phys. Rev. Lett.* **1997**, *79*, 1467−1470.
(9) Lang, C.; Bozyigit, D.; Eichler, C.; Steffen, L.; Fink, J. M.; Abdumalikov, A. A.; Baur, M.; Filipp, S.; da Silva, M. P.; Blais, A.; Wallraff, A. Observation of resonant photon blockade at microwave frequencies using correlation function measurements. *Phys. Rev. Lett.* **2011**, *106*, 243601.
(10) Rabl, P. Photon blockade effect in optomechanical systems. *Phys. Rev. Lett.* **2011**, *107*, 063601.
(11) Snijders, H. J.; Frey, J. A.; Norman, J.; Flayac, H.; Savona, V.; Gossard, A. C.; Bowers, J. E.; van Exter, M. P.; Bouwmeester, D.; Löffler, W. Observation of the unconventional photon blockade. *Phys. Rev. Lett.* **2018**, *121*, 043601.
(12) Vaneph, C.; Morvan, A.; Aiello, G.; Féchant, M.; Aprili, M.; Gabelli, J.; Estève, J. Observation of the unconventional photon blockade in the microwave domain. *Phys. Rev. Lett.* **2018**, *121*, 043602.
(13) Dhar, H. S.; Zens, M.; Krimer, D. O.; Rotter, S. Variational renormalization group for dissipative spin-cavity systems: periodic pulses of nonclassical photons from mesoscopic spin ensembles. *Phys. Rev. Lett.* **2018**, *121*, 133601.
(14) Huang, R.; Miranowicz, A.; Liao, J.-Q.; Nori, F.; Jing, H. Nonreciprocal photon blockade. *Phys. Rev. Lett.* **2018**, *121*, 153601.
(15) Li, B.; Huang, R.; Xu, X.; Miranowicz, A.; Jing, H. Nonreciprocal unconventional photon blockade in a spinning optomechanical system. *Photonics Res.* **2019**, *7*, 630−641.
(16) Liew, T. C. H.; Savona, V. Single photons from coupled quantum modes. *Phys. Rev. Lett.* **2010**, *104*, 183601.
(17) Radulaski, M.; Fischer, K. A.; Lagoudakis, K. G.; Zhang, J. L.; Vučković, J. Photon blockade in two-emitter-cavity systems. *Phys. Rev. A: At., Mol., Opt. Phys.* **2017**, *96*, 011801.
(18) Bamba, M.; Imamoğlu, A.; Carusotto, I.; Ciuti, C. Origin of strong photon antibunching in weakly nonlinear photonic molecules. *Phys. Rev. A: At., Mol., Opt. Phys.* **2011**, *83*, 021802.
(19) Carreño, J. C. L.; Casalengua, E. Z.; del Valle, E.; Laussy, F. P. Criterion for single photon sources. *arXiv* (Quantum Physics), October 2016, 1610.06126; https://arxiv.org/pdf/1610.06126.pdf (accessed 2016-10-19).
(20) Xu, X.-W.; Li, Y.-J. Antibunching photons in a cavity coupled to an optomechanical system. *J. Phys. B: At., Mol. Opt. Phys.* **2013**, *46*, 035502.
(21) Majumdar, A.; Bajcsy, M.; Rundquist, A.; Vučković, J. Loss-enabled sub-poissonian light generation in a bimodal nanocavity. *Phys. Rev. Lett.* **2012**, *108*, 183601.
(22) Zhou, Y. H.; Shen, H. Z.; Yi, X. X. Unconventional photon blockade with second-order nonlinearity. *Phys. Rev. A: At., Mol., Opt. Phys.* **2015**, *92*, 023838.
(23) Xu, X.-W.; Li, Y. Strong photon antibunching of symmetric and antisymmetric modes in weakly nonlinear photonic molecules. *Phys. Rev. A: At., Mol., Opt. Phys.* **2014**, *90*, 033809.
(24) Santhosh, K.; Bitton, O.; Chuntonov, L.; Haran, G. Vacuum Rabi splitting in a plasmonic cavity at the single quantum emitter limit. *Nat. Commun.* **2016**, *7*, 11823.
(25) Chikkaraddy, R.; de Nijs, B.; Benz, F.; Barrow, S. J.; Scherman, O. A.; Rosta, E.; Demetriadou, A.; Fox, P.; Hess, O.; Baumberg, J. J. Single-molecule strong coupling at room temperature in plasmonic nanocavities. *Nature* **2016**, *535*, 127.
(26) Liu, R.; Zhou, Z.-K.; Yu, Y.-C.; Zhang, T.; Wang, H.; Liu, G.; Wei, Y.; Chen, H.; Wang, X.-H. Strong light-matter interactions in single open plasmonic nanocavities at the quantum optics limit. *Phys. Rev. Lett.* **2017**, *118*, 237401.
(27) Ojambati, O. S.; Chikkaraddy, R.; Deacon, W. D.; Horton, M.; Kos, D.; Turek, V. A.; Keyser, U. F.; Baumberg, J. J. Quantum electrodynamics at room temperature coupling a single vibrating molecule with a plasmonic nanocavity. *Nat. Commun.* **2019**, *10*, 1−7.
(28) Gupta, S. N.; Bitton, O.; Neuman, T.; Esteban, R.; Chuntonov, L.; Aizpurua, J.; Haran, G. Complex plasmon-exciton dynamics revealed through quantum dot light emission in a nanocavity. *arXiv* (Mesoscale and Nanoscale Physics), September 2019, 1909.10231; https://arxiv.org/ftp/arxiv/papers/1909/1909.10231.pdf (accessed 2020-04-21).
(29) Xiong, X.; You, J.-B.; Bai, P.; Png, C. E.; Zhou, Z.-K.; Wu, L. Ultrastrong coupling in single plexcitonic nanocubes. *Nanophotonics* **2020**, *9*, 257−266.
(30) Zengin, G.; Wersäll, M.; Nilsson, S.; Antosiewicz, T. J.; Käll, M.; Shegai, T. Realizing strong light-matter interactions between single-nanoparticle plasmons and molecular excitons at ambient conditions. *Phys. Rev. Lett.* **2015**, *114*, 157401.
(31) Cuadra, J.; Baranov, D. G.; Wersall, M.; Verre, R.; Antosiewicz, T. J.; Shegai, T. Observation of tunable charged exciton polaritons in hybrid monolayer WS2- plasmonic nanoantenna system. *Nano Lett.* **2018**, *18*, 1777−1785.
(32) Steck, D. A. *Quantum and Atom Optics*, rev. 0.13.1; UO Atom Optics: 2007; http://atomoptics-nas.uoregon.edu/~dsteck/teaching/quantum-optics/quantum-optics-notes.pdf (accessed 2020-4-29).
(33) Aghamalyan, D.; You, J.-B.; Chu, H.-S.; Png, C. E.; Krivitsky, L.; Kwek, L. C. Tunable quantum switch realized with a single Λ-level atom coupled to the microtoroidal cavity. *Phys. Rev. A: At., Mol., Opt. Phys.* **2019**, *100*, 053851.
(34) Berthel, M.; Mollet, O.; Dantelle, G.; Gacoin, T.; Huant, S.; Drezet, A. Photophysics of single nitrogen-vacancy centers in diamond nanocrystals. *Phys. Rev. B: Condens. Matter Mater. Phys.* **2015**, *91*, 035308.
(35) Hamsen, C.; Tolazzi, K. N.; Wilk, T.; Rempe, G. Two-photon blockade in an atom-driven cavity QED system. *Phys. Rev. Lett.* **2017**, *118*, 133604.
(36) Klaas, M.; Schlottmann, E.; Flayac, H.; Laussy, F. P.; Gericke, F.; Schmidt, M.; Helversen, M. v.; Beyer, J.; Brodbeck, S.; Suchomel, H.; Höfling, S.; Reitzenstein, S.; Schneider, C. Photon-number-resolved measurement of an exciton-polariton condensate. *Phys. Rev. Lett.* **2018**, *121*, 047401.
(37) Deng, H.; Solomon, G. S.; Hey, R.; Ploog, K. H.; Yamamoto, Y. Spatial Coherence of a polariton condensate. *Phys. Rev. Lett.* **2007**, *99*, 126403.
(38) Kasprzak, J.; Richard, M.; Baas, A.; Deveaud, B.; André, R.; Poizat, J.-P.; Dang, L. S. Second-order time correlations within a polariton Bose−Einstein condensate in a CdTe microcavity. *Phys. Rev. Lett.* **2008**, *100*, 067402.
(39) Horikiri, T.; Schwendimann, P.; Quattropani, A.; Höfling, S.; Forchel, A.; Yamamoto, Y. Higher order coherence of exciton-polariton condensates. *Phys. Rev. B: Condens. Matter Mater. Phys.* **2010**, *81*, 033307.
(40) Aßmann, M.; Veit, F.; Bayer, M.; van der Poel, M.; Hvam, J. M. Higher-order photon bunching in a semiconductor microcavity. *Science* **2009**, *325*, 297−300.
(41) Xu, D.; Xiong, X.; Wu, L.; Ren, X.-F.; Png, C. E.; Guo, G.-C.; Gong, Q.; Xiao, Y.-F. Quantum plasmonics: new opportunity in fundamental and applied photonics. *Adv. Opt. Photonics* **2018**, *10*, 703−756.

(42) Zhou, Z.-K.; Liu, J.; Bao, Y.; Wu, L.; Png, C. E.; Wang, X.-H.; Qiu, C.-W. Quantum plasmonics get applied. *Prog. Quantum Electron.* **2019**, *65*, 1−20.

(43) Qian, C.; Wu, S.; Song, F.; Peng, K.; Xie, X.; Yang, J.; Xiao, S.; Steer, M. J.; Thayne, I. G.; Tang, C.; et al. Two-photon Rabi splitting in a coupled system of a nanocavity and exciton complexes. *Phys. Rev. Lett.* **2018**, *120*, 213901.

(44) Schwartz, T.; Hutchison, J. A.; Genet, C.; Ebbesen, T. W. Reversible switching of ultrastrong light-molecule coupling. *Phys. Rev. Lett.* **2011**, *106*, 196405.

(45) Xiao, Y.-F.; Liu, Y.-C.; Li, B.-B.; Chen, Y.-L.; Li, Y.; Gong, Q. Strongly enhanced light-matter interaction in a hybrid photonic-plasmonic resonator. *Phys. Rev. A: At., Mol., Opt. Phys.* **2012**, *85*, 031805.

(46) Peng, P.; Liu, Y.-C.; Xu, D.; Cao, Q.-T.; Lu, G.; Gong, Q.; Xiao, Y.-F.; et al. Enhancing coherent light-matter interactions through microcavity-engineered plasmonic resonances. *Phys. Rev. Lett.* **2017**, *119*, 233901.

(47) Gurlek, B.; Sandoghdar, V.; Martín-Cano, D. Manipulation of quenching in nanoantenna−emitter systems enabled by external detuned cavities: a path to enhance strong-coupling. *ACS Photonics* **2018**, *5*, 456−461.

(48) Bisht, A.; Cuadra, J.; Wersall, M.; Canales, A.; Antosiewicz, T. J.; Shegai, T. Collective strong light-matter coupling in hierarchical microcavity-plasmon-exciton systems. *Nano Lett.* **2019**, *19*, 189−196.

https://dx.doi.org/10.1021/acs.nanolett.0c01562
Nano Lett. 2020, 20, 4645−4652